Multiobjective optimization of efficiency, head, free passage and vibrations of two blade impeller for sewage pump with stationary front shroud

Wielokryterialna optymalizacja sprawności, wysokości podnoszenia, swobodnego przelotu i poziomu wibracji pompy ściekowej z wirnikiem dwułopatowym współpracującym z nieruchomą tarczą przednią

MIKOŁAJ SITNIEWSKI, JANUSZ SKRZYPACZ, PRZEMYSŁAW SZULC, MARCIN JANCZAK, WITOLD LORENZ

DOI 10.36119/15.2025.3.7

This paper presents a multiobjective optimization procedure for a two-blade impeller in a sewage pump with a stationary front shroud. The optimization variables were the wrap angles on the front and back shroud, while the meridional cross-section and volute remained constant. The objective was to maximize efficiency, head, and free passage (e.g., minimizing blockage) while minimizing vibrations by reducing radial forces. A full factorial design with five levels was used for CFD (computational fluid dynamics) calculations. After selecting the optimal design, the results of initial and optimized impeller were validated experimentally. Numerical and experimental results demonstrated good agreement. The optimized impeller showed improvements: head increased by 38,4%, efficiency by 9,5%, and free passage by 8,3%. While CFD calculations predicted a reduction in averaged radial forces, vibration measurements on volute indicated an increase for the optimized impeller by 46,1%. This discrepancy suggests that radial forces may not be the primary factor influencing vibrations in this specific pump configuration. The findings of this study contribute to the development of more efficient and reliable sewage pumps.
Keywords: sewage pump, optimization, two blade impeller, radial forces, vibrations

Artykuł przedstawia procedurę optymalizacji wielokryterialnej dwułopatkowego wirnika w pompie ściekowej z nieruchomą tarczą przednią. Zmiennymi optymalizacyjnymi były kąty opasania na tarczy przedniej i tarczy tylnej, podczas gdy przekrój meridionalny i spiralny korpus zbiorczy pozostały stałe. Celem było zmaksymalizowanie sprawności, wysokości podnoszenia i swobodnego przelotu przy jednoczesnej minimalizacji poziomu wibracji poprzez redukcję sił promieniowych. Do obliczeń CFD (computational fluid dynamics) zastosowano pełny plan czynnikowy z pięcioma poziomami. Po wybraniu optymalnego projektu, parametry pompy z wirnikiem początkowym i zoptymalizowanym zostały zweryfikowane eksperymentalnie. Wyniki numeryczne i eksperymentalne wykazały dobrą zgodność. Zoptymalizowany wirnik wykazał poprawę: wysokość podnoszenia wzrosła o 38,4%, sprawność o 9,5% i swobodny przelot o 8,3%. Podczas gdy obliczenia CFD przewidywały redukcję uśrednionych sił promieniowych, pomiary poziomu wibracji na spirali wskazały na wzrost dla zoptymalizowanego wirnika o 46,1%. Ta rozbieżność sugeruje, że siły promieniowe mogą nie być głównym czynnikiem wpływającym na poziom wibracji w tej konfiguracji pompy. Wyniki przedstawionych badań przyczyniają się do rozwoju pomp ściekowych o lepszych parametrach energetycznych i użytkowych.
Słowa kluczowe: pompa ściekowa, optymalizacja, wirnik dwułopatowy, siły promieniowe, drgania

Introduction

Centrifugal sewage pump failures can have significant economic and environmental consequences due to the continuous flow of sewage and the disruptions caused by necessary repairs. These repairs often involve dismantling the pipeline and pump, removing blockages, and reassembly, all of which require specialized personnel and incur significant costs. Therefore, a crucial design consideration for sewage pumps is resistance to blockages caused by materials present in the sewage. While semi-open vortex impellers offer some blockage resistance, they suffer from low efficiency. Pre-shredders can mitigate blockages but are often expensive and impractical for high-capacity pumps. In such cases, reducing the number of impeller blades (e.g., using two-blade or single-blade designs) increases free passage, a critical parameter for handling solids in contaminated liquids such as sewage.

Free passage is defined as the maximum diameter of a sphere that can pass unobstructed through the pump's hydraulic system. However, the primary cause of impeller clogging in sewage pumps is often not large solids, but rather fibrous materials such as towels, clothes, and diapers [1], which tend to accumulate on the impeller inlet edge.

To mitigate this, many sewage pumps incorporate a stationary front shroud with cutting grove (those pumps are often called a "contrablock"), which grinds fibrous materials and prevents their accumulation on the impeller blades. While this significantly improves blockage resistance, it can introduce minor efficiency losses due to increased leakage flows between the stationary shroud and the rotating impeller. Studies by Souza et al. [2] and Caruso et al. [3] have investigated

mgr inż. Mikołaj Sitniewski https://orcid.org/0009-0001-3081-8802, dr hab. inż. Janusz Skrzypacz https://orcid.org/0000-0003-2021-3487, dr inż. Przemysław Szulc https://orcid.org/0000-0003-1753-9611 – Politechnika Wrocławska
dr inż. Marcin Janczak, dr inż. Witold Lorenz https://orcid.org/0009-0005-5274-7127 – Hydro Vacuum S.A.
Adres do korespondencji/Corresponding author: mikolaj.sitniewski@pwr.edu.pl

the impact of the gap between the impeller and shroud on the performance of single-blade impellers. These studies demonstrate that a well-maintained gap minimizes efficiency losses, emphasizing the importance of regular gap adjustments throughout the pump's lifecycle. Yang Y. et al. [4] further investigated the effects of tip clearance in three-blade impellers, describing the formation of vortices due to leakage flows. Their research suggests that adjusting the clearance can influence pump performance. Overall, while the use of a stationary front shroud may slightly decrease efficiency, its benefits in preventing blockages make it a valuable component in many sewage pump designs.

Reducing the number of blades is beneficial for increasing free passage, but it presents challenges during the design stage. Standard design theories often assume uniform flow patterns, which are not present in two-blade or single-blade impellers. Minimizing the number of blades is associated with several issues, including high levels of fluid-induced vibrations that increase as the blade count decreases. Furthermore, vibrations induced by the fluid in one-blade and two-blade impellers can overlap with vibrations caused by mechanical faults, such as unbalance, bearing misalignment, and cocked bearings, at synchronous (1x) and twice synchronous (2x) frequencies. Tan L. et al. [5] investigated the influence of blade wrap angle on the hydrodynamic radial force of a single-blade impeller. They found that increasing the wrap angle improved head and efficiency but narrowed the high-efficiency operating range. The radial forces were strongly dependent on the wrap angle, with a significant decrease observed as the wrap angle increased. However, this study primarily focused on energy characteristics and did not include experimental validation of the predicted radial forces or vibration levels. Wang C. et al. [6] explored the impact of rotation center eccentricity on radial force in a single-blade impeller, aiming to mitigate large fluctuating forces. While they found that eccentricity can effectively reduce radial forces, their study also lacked experimental validation of the predicted force reductions and their impact on vibration levels. Kim et al. [7, 8, 9, 10, 11] and Nguyen et al. [12] optimized a single-channel impeller to improve efficiency and reduce unsteady radial forces, thereby mitigating flow-induced vibrations. Their optimization process involved modifying the impeller and volute shapes using Stepanoff's theory and employing a hybrid particle swarm optimization and genetic algorithm coupled with surrogate modelling. CFD simulations, including both steady and unsteady Reynolds-Averaged Navier-Stokes equations, were used to evaluate the designs. The optimized design demonstrated improved efficiency and reduced variable radial forces, with experimental results confirming increased efficiency and decreased vibration at the blade passing frequency (BPF). Tan L. et al. [13] investigated a single-blade impeller using numerical simulations, performance tests, and particle image velocimetry (PIV). Their study focused on characterizing secondary flows within the impeller, including jet-wake structures at the impeller outlet, which are known to contribute to losses and induce vibrations. Cui et al. [14] investigated the correlation between radial forces, total entropy generation (TEG), entropy generation rate (EGR), and flow-induced vibrations in a single-stage, low-speed centrifugal pump with a 5-blade impeller across various operating conditions. They employed CFD and fluid-structure interaction (FSI) analyses and validated their numerical model through experimental measurements of vibrations and energy parameters. The results demonstrated that radial force, TEG, EGR, and vibration levels were minimized at the pump's optimal efficiency point and increased as operating conditions deviated from this point. This finding supports the use of radial force, TEG, and EGR as indicators of flow-induced pump vibrations. The study also confirmed the previously observed phenomenon of changes in radial force vector direction with variations in efficiency. Pei et al. [15] utilized FSI simulations with strong two-way coupling to investigate unsteady flow-induced impeller oscillations in a single-blade pump under off-design conditions. To validate their CFD-FSI model, they employed proximity sensors to measure shaft and impeller deformations in the radial direction and conducted experiments under various operating conditions. While the strain values obtained from FSI and experiments showed good agreement, a phase shift of half a shaft revolution was observed between the predicted and measured strain values. Song et al. [16] investigated pressure oscillations and radial forces in centrifugal pumps with single and double-suction impellers. Their results demonstrated good agreement between CFD simulations and experimental data in terms of Q-H characteristics and pressure oscillations around the spiral circumference. Furthermore, the study showed that double-suction impellers effectively reduce pressure oscillations and radial forces. It is important to note that vibration problems are not limited to single-blade impellers. Two-blade impellers are also susceptible to significant vibration levels, and existing research on this specific configuration is relatively limited. Ma et al. [17] conducted a multi-objective optimization of a two-blade sewage pump impeller, focusing on maximizing free passage, head, and efficiency. The optimization variables included impeller blade angle and volute cross-sectional area, determined using Stepanoff's theory. The optimization process utilized CFD methods in conjunction with a machine-learning-based artificial neural network. While the study achieved improvements in the target hydraulic parameters, it did not explicitly consider flow-induced vibrations, a critical factor for two-blade impeller designs. Ren Y. et al. [18] employed a genetic algorithm to optimize a two-blade sewage pump impeller, considering head, efficiency, and average wear depth as optimization objectives. Their approach utilized a coupled Computational Fluid Dynamics-Discrete Element Method (CFD-DEM) simulation.

As demonstrated by these previous studies, effective methodologies for designing two-blade impellers that simultaneously achieve increased free passage, high efficiency, and reduced vibrations are currently lacking. This research addresses this gap by presenting a multi-objective optimization framework for two-blade impellers based on logarithmic curves (curves with a constant beta angle).

Methods

A Hydro-Vacuum S.A. pump model FZF.5.21, equipped with a DN 150 inlet and a DN 125 outlet in accordance with the EN-1092 standard, was used for the tests. The impeller was modified, while the mechanical drive, volute, and stationary front shroud remained unchanged. Figure 1 illustrates the

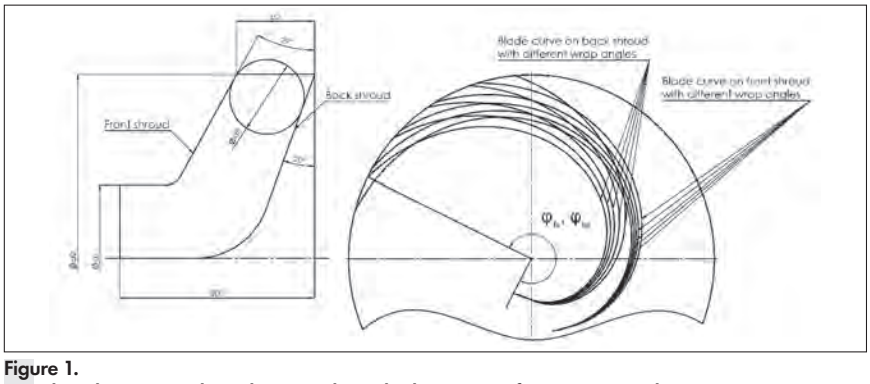

Figure 1.
Meridional section and axial view with marked maximum free passage value
Rysunek 1. Przekrój merydionalny i widok na płaszczyznę prostopadłą do osi z zaznaczoną maksymalną wartością swobodnego przelotu

meridional and axial view of the impeller. The geometric parameters are summarized in Table 1.

Table 1. Main geometrical parameters of impeller
Tabela 1. Główne wielkości geometryczne wirnika

Main geometrical parameters:	Value:
Inlet diameter of impeller d_1	150 mm
Outlet diameter of impeller d_2	375 mm
Outlet width of the impeller b_2	80 mm
Blade wrap angle on front shroud φ_{fs}	To be defined
Blade wrap angle on back shroud φ_{bs}	To be defined
Diameter of free passage d_{fr}	To be optimized

The research conducted by [19] indicates that logarithmic curves offer a superior blade profile for centrifugal pump impellers. Therefore, this study adopts the logarithmic curve as the basis for blade design. The equation describing a blade with a constant angle along the curve is:

$$r = ae^{b\varphi} \quad (1),$$

where r is radius, a, b are constants, φ is angle.

Literature review presented above and preliminary tests indicate that the wrap angle is a critical parameter for impeller design. This analysis investigates the influence of wrap angle, implemented using logarithmic spirals with a constant curve angle. To prevent fibrous materials from accumulating on the impeller's inlet edge, the edge must be appropriately shaped, inclined towards the stationary front disc. Our previous preliminary research demonstrated that an edge that does not effectively deflect solids towards the grinding disc can lead to the accumulation of fibrous materials. Therefore, in this analysis, the inlet edge geometry was kept constant, and the logarithmic curve on the front disc was shifted by 30 degrees to achieve the desired inlet edge inclination.

A full factorial design was employed to plan the experiment, with five levels for front shroud wrap angles: 205°, 220°, 235°, 250°, 265° and five levels for back shroud wrap angle 190°, 205°, 220°, 235°, 250°. This resulted in 25 simulations (5 levels x 5 levels) to be conducted at the optimal operating point of 340 m^3/h.

Figure 2 shows the boundary conditions for CFD calculations. CFD calculations were performed using the Reynolds-Averaged Navier-Stokes equations with the SST k-ω turbulence model. All simulations were executed on a computing cluster using Fluent 2024 R1 software. Initially, 6,000 iterations of steady-state calculations were performed, requiring approximately 12 hours. Subsequently, transient simulations were conducted over three impeller revolutions with a time step of 0.0001149 seconds, corresponding to a rotation angle of 1 degree at a rotational speed

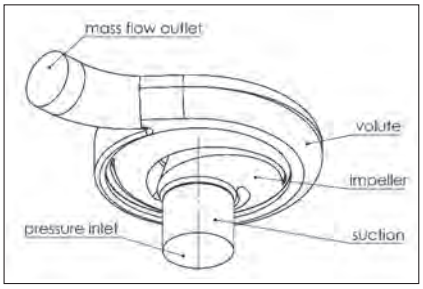

Figure 2.
Boundary conditions and cell zones for CFD calculations
Rysunek 2. Warunki brzegowe i objętości brył w obliczeniach CFD

of 1450 RPM. This stage required approximately 48 hours of computation time. The use of a computing cluster facilitated the efficient evaluation of 25 different geometries without compromising mesh quality. The gap between the disc and the impeller was neglected in the CFD simulations. Numerical calculations did not incorporate frictional losses associated with bearings, mechanical seals, and the rotating rear disc, as these components were not explicitly modelled. Consequently, a mechanical loss factor of 0.88 was applied as a multiplier to the pump efficiency η.

A grid independence study was conducted to ensure that the CFD results were not influenced by mesh resolution. The mesh dependence was evaluated at the best efficiency point (340 m^3/h). Figure 3 a) illustrates the

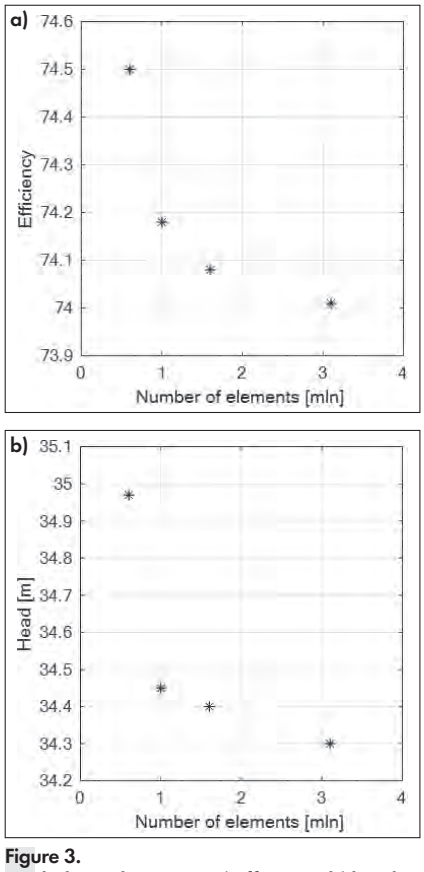

Figure 3.
Mesh dependency test: a) efficiency, b) head
Rysunek 3. Test wpływu wielkości siatki na: a) sprawność, b) wysokość podnoszenia

variation of efficiency with the number of mesh cells, while Figure 3 b) shows the corresponding variation in head. Based on these results, a mesh with 3.1 million elements was selected for the subsequent analyses. Cross sectional of that mesh with inflation layer is presented on Figure 4.

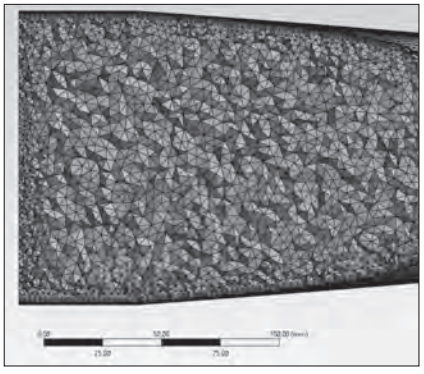

Figure 4.
Cross sectional of volute mesh
Rysunek 4. Przekrój siatki obliczeniowej spiralnego kanału zbiorczego

In addition to efficiency, head, and radial force, which were evaluated using CFD, the free passage of each impeller was assessed using CAD software. The meridional cross-section limits the free passage to 78 mm, as illustrated in Figure 1.

Following an approach described in the literature review [5, 6, 8, 9, 10, 11, 12], the optimization strategy focused on minimizing vibrations by minimizing the radial forces acting on the impeller. The optimization objectives included: head, efficiency, free passage, and radial force. The weighted criteria method was employed for optimization, where each objective was first standardized according to Equation (2). Each objective was assigned an equal weight of 0.25.

$$z = \frac{x - \mu}{\sigma} \quad (2)$$

z – standardized variable
x – non-standardized variable
μ – mean of the population
σ – standard deviation of the population

Results

Figure 5-8 present the results for the head, the efficiency, free passage and the radial force as a functions of the front and back shroud wrap angles. The results indicate that the head is most significantly influenced by the equality of front and back shroud wrap angles, with the specific values of these angles having a lesser impact. Figure 6 shows that impeller efficiency generally increases with increasing wrap angles on both the front and back shroud. The free passage values increase with decreasing wrap angles, but this trend is constrained by the maximum allowable value determined by the

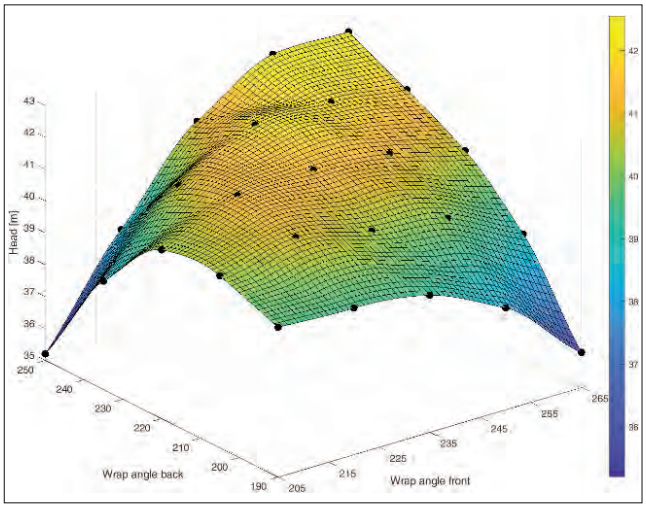

Figure 5.
3D plot of head as a function of wrap angles on front and back shroud
Rysunek 5. Wykres 3D wysokości podnoszenia w funkcji kąta opasania na tarczy przedniej i tarczy tylnej

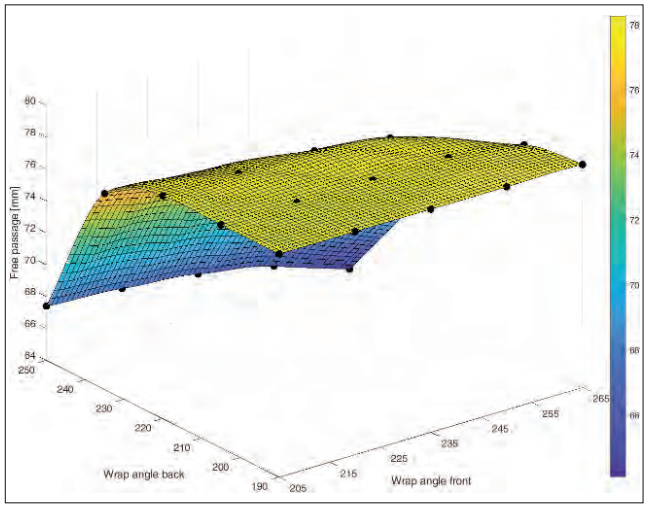

Figure 7.
3D plot of free passage value as a function of wrap angles on front and back shroud
Rysunek 7. Wykres 3D swobodnego przelotu w funkcji kąta opasania na tarczy przedniej i tarczy tylnej

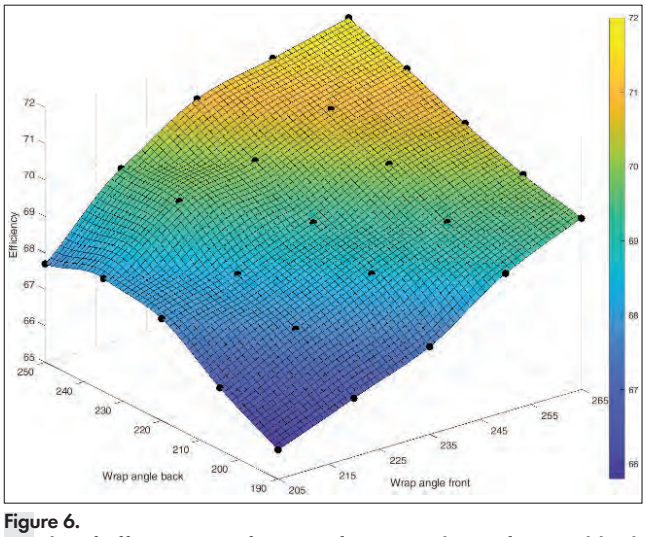

Figure 6.
3D plot of efficiency as a function of wrap angles on front and back shroud
Rysunek 6. Wykres 3D sprawności w funkcji kąta opasania na tarczy przedniej i tarczy tylnej

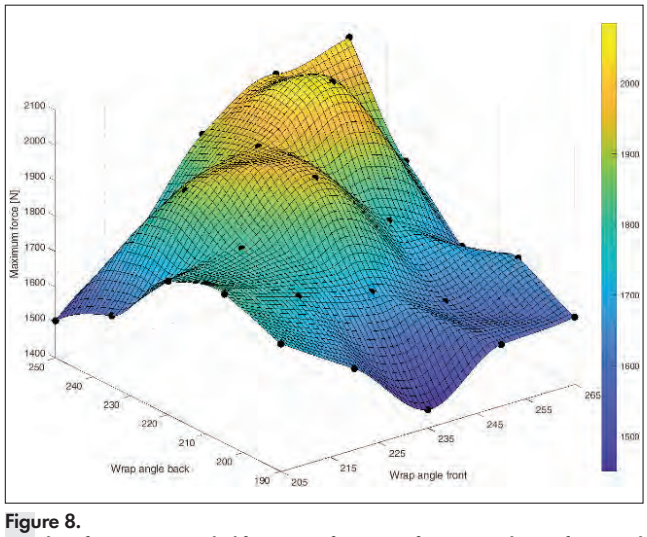

Figure 8.
3D plot of maximum radial force as a function of wrap angles on front and back shroud
Rysunek 8. Wykres 3D maksymalnej siły promieniowej w funkcji kąta opasania na tarczy przedniej i tarczy tylnej

meridional cross-section. The radial force exhibits a trend similar to head, but since minimizing radial force is a key objective, these trends create a conflicting design requirement.

Figure 9 illustrates the optimization function after standardizing the variables and summing the weighted criteria. The optimization function reaches a maximum at a front wrap angle of 250 degrees and a back wrap angle of 216 degrees. The optimized impeller was then re-simulated using CFD to compare its performance with the initial impeller designs. CFD results were further validated through experimental testing. Figure 10 presents a comparison of radial forces for the initial and optimized impellers during one revolution, demonstrating a 30% reduction in radial force for the optimized design.

To validate the CFD calculations, the optimized impeller design was 3D printed using FDM technology. The initial design was

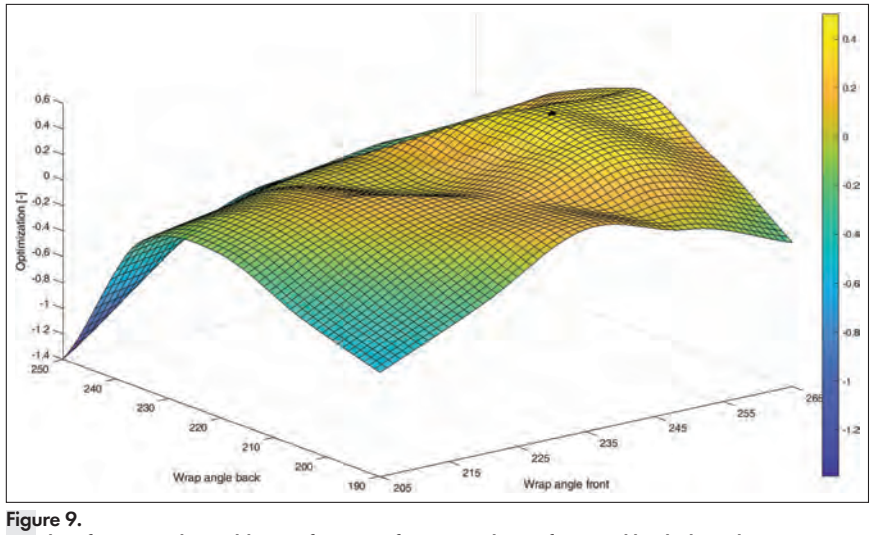

Figure 9.
3D plot of optimized variable as a function of wrap angles on front and back shroud
Rysunek 9. Wykres 3D funkcji optymalizacji w zależności od kąta opasania na tarczy przedniej i tarczy tylnej

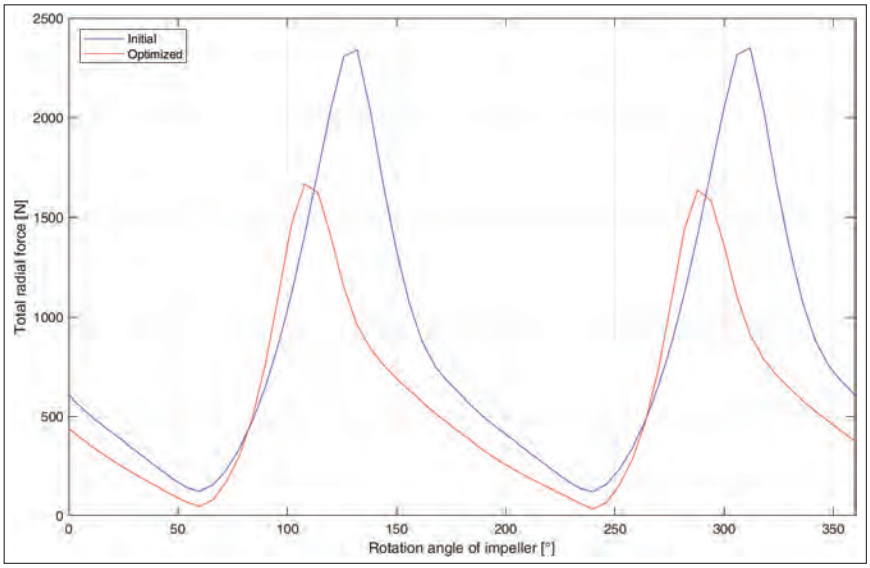

Figure 10.
Radial forces of initial and optimized impeller during one rotation at nominal capacity (340 m^3/h)
Rysunek 10. Siły promieniowe wirnika początkowego i zoptymalizowanego podczas jednego obrotu przy wydajności optymalnej (340 m^3/h)

manufactured as a cast iron impeller. These impellers were then integrated into a standard FZ.5 pump produced by Hydro-Vacuum S.A. with with a three-phase electric motor with a power of 110 kW and a rotational speed of 1480 RPM. Figure 11 presents photographs of the tested impellers. Figure 12 shows the tested pump with discharge and suction pipelines on the test stand. The gap between the impeller and the grinding disc in the impellers was adjusted and was within the range of 0.2-0.4 mm.

Figure 11.
Impellers for experiments – left optimized, right initial
Rysunek 11. Wirniki do badań – z lewej strony zoptymalizowany, z prawej strony początkowy

Figure 12.
Tested pump with discharge and suction pipelines on the test rig
Rysunek 12. Badana pompa z rurociągami: tłocznym i ssawnym

Figure 13 and Figure 14 illustrates the Q-H and Q-η curves for the initial and optimized impellers. The presented optimization procedure effectively ensured that the maximum efficiency was achieved at the target flow rate of 340 m^3/h.

It is well-known that reducing the pump's specific speed generally leads to a decrease in achievable maximum efficiency. However, in this case, increasing the head, which consequently reduces the specific speed, resulted in an increase in efficiency.

The omission of leakage between the impeller and the front shroud resulted in a marginal shift of optimal efficiency toward lower values for both the initial and optimized impeller.

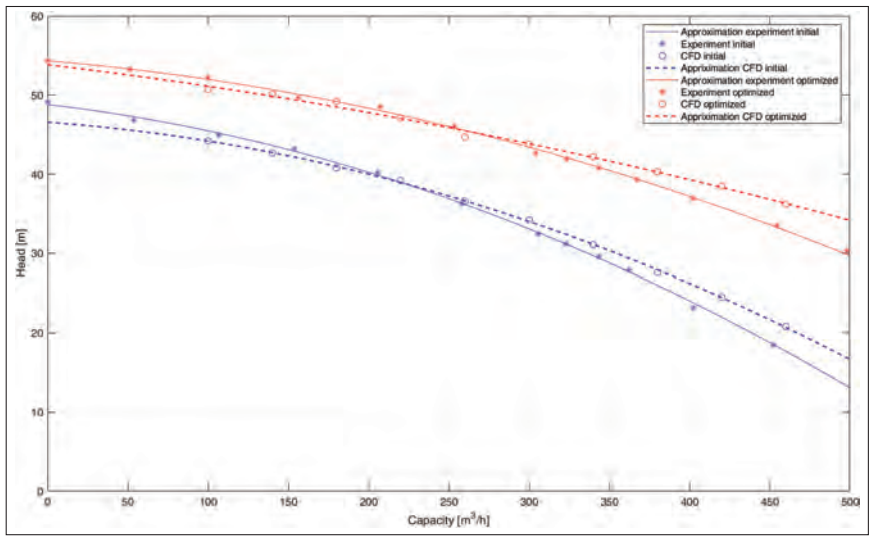

Figure 13.
Q-H curve of initial and optimized impeller – CFD calculations and experiment
Rysunek 13. Wykres wysokości podnoszenia w zależności od wydajności dla wirnika początkowego i optymalnego – obliczenia CFD i eksperyment

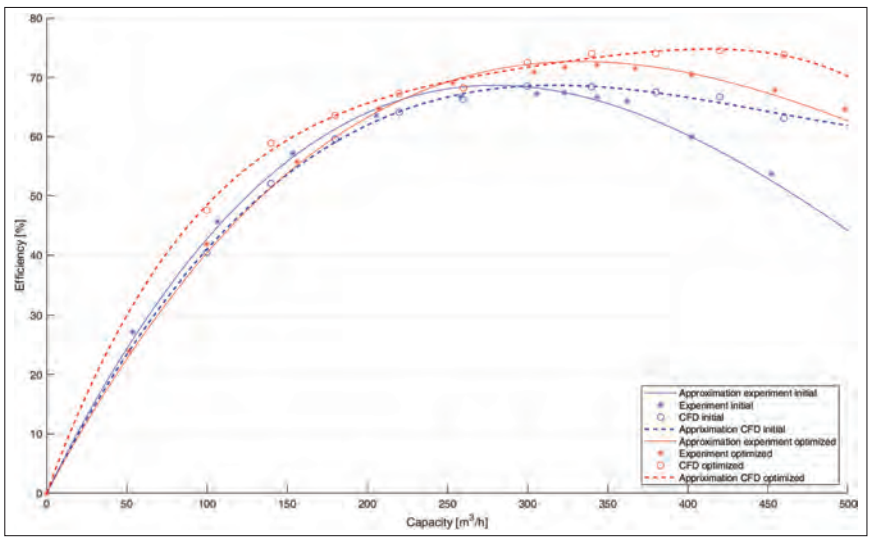

Figure 14.
Q-η curve of initial and optimized impeller – CFD calculations and experiment
Rysunek 14 Wykres sprawności w zależności od wydajności dla wirnika początkowego i optymalnego – obliczenia CFD i eksperyment

Table 2. Experimental and CFD results of head for initial and optimized impeller
Tabela 2. Wyniki eksperymentalne i CFD wysokości podnoszenia dla wirnika początkowego i optymalnego

Head [m]	Initial			Optimized		
	H cfd	H exp	Relative error	H cfd	H exp	Relative error
260 m^3/h	36,6	36,2	1,09%	45,5	45,5	0%
340 m^3/h (BEP)	31,1	29,7	4,50%	42,1	41,1	2,43%
420 m^3/h	24,5	22,0	10,20%	38,3	35,8	6,53%

Table 3 Experimental and CFD results of efficiency for initial and optimized impeller
Tabela 3. Wyniki eksperymentalne i CFD sprawności dla wirnika początkowego i optymalnego

Efficiency	Initial			Optimized		
	η cfd	η exp	Relative error	η cfd	η exp	Relative error
260 m^3/h	67,2	68,4	-1,79%	71,2	70,0	1,69%
340 m^3/h (BEP)	68,5	66,4	3,07%	72,5	72,6	-0,14%
420 m^3/h	65,7	57,5	12,48%	73,4	69,6	5,18%

Table 2 and 3 present a comparison of numerically simulated and experimentally measured head and efficiency values at three flow rates: 260, 340, and 420 m^3/h. The tables also include the relative error of the numerical calculations. The maximum relative error of 12.48% was observed in the impeller efficiency at the highest flow rate of 420 m^3/h. However, for the subsequent analysis, the point of best efficiency (BEP) is of greater significance. At the BEP, the relative error remained below 5% in all cases. Discrepancies between the computational fluid dynamics (CFD) results and the experimental data are attributable, in part, to the surface roughness of the hydraulic channels within the spiral casing and the impellers. The lower roughness of the FDM-manufactured impeller, coupled with the alignment of layer lines with the primary flow direction within most of the channel, contributed to the observed reduction in error for this specific impeller.

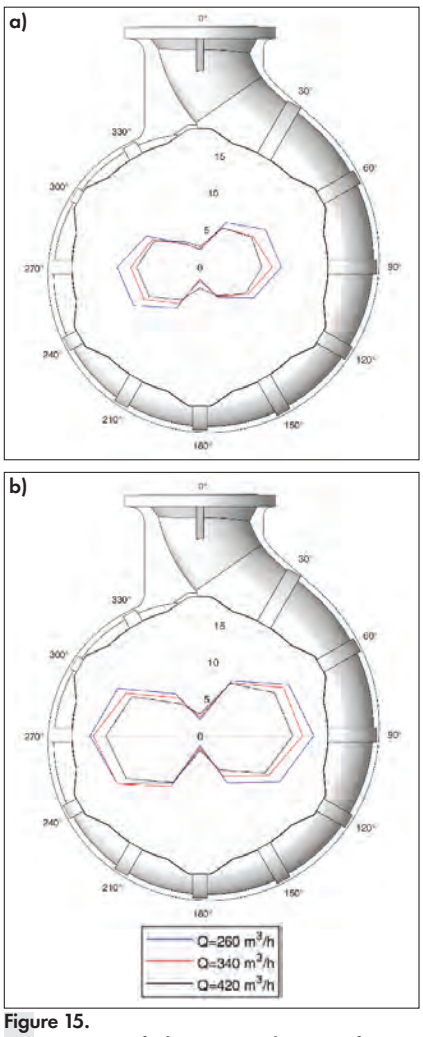

Figure 15.
Measurement of vibrations on the circumference of the volute – V_{rms} values [mm/s]: a) initial, b) optimized
Rysunek 15. Wyniki pomiaru poziomu drgań na obwodzie spiralnego korpusu zbiorczego – wartości V_{rms} [mm/s]: a) początkowy, b) optymalny

Vibration measurements were conducted on the circumference of the casing body for both the initial and optimized impellers at three flow rates: 260 m^3/h, 340 m^3/h, and 420 m^3/h. The results, presented in Figure 15, show root-mean-square (RMS) vibration levels. For all measurements, the dominant frequency was the blade passing frequency (BPF), which in this case is 50 Hz due to the two-bladed impeller.

An unexpected observation was an increase in vibration levels on the circumference of pump discharge casing for the optimized impeller despite the lower radial forces predicted by CFD calculations. Furthermore, both the initial and optimized impellers exhibited the lowest vibration levels at 420 m^3/h. This contradicts the general understanding of centrifugal pump behavior, which typically observes minimum vibrations at the point of optimal efficiency. The lowest vibration levels were observed in the plane of the discharge and suction pipelines, potentially due to the greater stiffness of the system in that direction compared to the perpendicular direction.

Summary

This paper presents a multi-objective optimization method for two-blade sewage pump impellers, considering free passage, maximizing efficiency, and minimizing vibrations expressed in terms of radial forces. Stationary and transient CFD calculations were performed for a full grid sampling of two parameters: front and back wrap angle, each with five levels, to determine the optimal combination of these parameters. The performance of the initial and optimized impellers was validated through energy tests (Q-H and Q-η curves) and vibration measurements.

The optimization process resulted in an improvement in efficiency, head and free passage. However, the expected reduction in vibrations was not observed. This discrepancy could be attributed to errors in the CFD simulations, inaccuracies in the vibration measurements, or a more complex relationship between radial forces and actual vibration levels than initially anticipated.

Despite the challenges in minimizing vibrations, this research provides a foundation for a novel approach to designing sewage pump impellers with enhanced free passage and improved hydraulic performance. Future research should include experimental measurements of radial forces acting on the impeller designs and further validation of the CFD results. If the CFD results are accurate, identifying and refining a suitable vibration indicator within the CFD simulations will be crucial for predicting vibration intensity more effectively.

Created using resources provided by Wroclaw Centre for Networking and Supercomputing (http://wcss.pl)

LITERATURE

[1] Isono M, Nohmi M, Uchida H, Kawai M, Kudo H, Kawahara T, Miyagawa K, Saito S. An experimental study on pump clogging. IOP Conference Series: Earth and Environmental Science. 2014;22. doi:10.1088/1755-1315/22/1/012009.
[2] Souza B, Daly J, Niven A, Frawley P. Numerical Simulation of Transient flow through Single Blade Centrifugal Pump Impellers with Tipgap Leakage. Proceedings of the 4th WSEAS International Conference on Fluid Mechanics and Aerodynamics. August 21-23, 2006. Elounda, Greece.
[3] Caruso F, Meskell C. Effect of the axial gap on the energy consumption of a single-blade wastewater pump. Proceedings of the Institution of Mechanical Engineers, Part A: Journal of Power and Energy. 2020;235(3):432-439. doi:10.1177/0957650920927366.
[4] Yang Y, Zhou L, Bai L, Xu H, Lv W, Shi W, Wang H. Numerical Investigation of Tip Clearance Effects On the Performance and Flow Pattern within a Sewage Pump. Journal of Fluids Engineering. 2022;144(8):081202. doi:10.1115/1.4053649.
[5] Tan L, Yang Y, Shi W, Chen C, Xie Z.s. Influence of Blade Wrap Angle on the Hydrodynamic Radial Force of Single Blade Centrifugal Pump. Applied Sciences. 2021;11(19):9052. doi:10.3390/app11199052.
[6] Wang C, Tan L, Shi W, Chenm C, Francis E. Research on Influence of Rotation Center Eccentricity on Radial Force of Single-Blade Centrifugal Pump. Water. 2022;14:2252. doi:10.3390/w14142252
[7] Kim J-H, Cho B-M, Kim Y-S, Choi Y-S, Kim K-Y, Kim J-H, Cho Y. Optimization of a Single-

-Channel Pump Impeller for Wastewater Treatment. International Journal of Fluid Machinery and Systems. 2016;9:370-381. doi:10.5293/IJFMS.2016.9.4.370.

[8] Kim J-H, Ma S-B, Kim S, Choi Y-S, Kim K-Y. Design and Verification of a Single-Channel Pump Model based on a Hybrid Optimization Technique. Processes. 2019;7(10):747. doi:10.3390/pr7100747

[9] Kim J-H, Choi Y-S. State-of-the-Art Design Technique of a Single-Channel Pump for Wastewater Treatment. Wastewater and Water Quality. 2017. doi:10.5772/intechopen.75171.

[10] Kim J-H, Ma S-B, Choi Y-S, Kim K-Y. Simultaneous Optimization of Impeller and Volute of a Single-channel Pump for Wastewater Treatment. International Journal of Fluid Machinery and Systems. 2019;12:99-108. doi:10.5293/IJFMS.2019.12.2.099.

[11] Kim J-H, Song W-G, Choi Y-S, Lee K-Y, Ma S-B, Kim K-Y. Three-objective optimization of a single-channel pump for wastewater treatment. IOP Conference Series: Earth and Environmental Science. 2019;240:032010 doi:10.1088/1755-1315/240/3/032010.

[12] Nguyen D-A, Roh M-S, Kim S, Kim J-H. Hydrodynamic and radial force characteristics with design of a single-channel pump for wastewater treatment based on the similarity law. Process Safety and Environmental Protection. 2023;170:1137-1150. doi:10.1016/j.psep.2022.12.090.

[13] Tan L, Wang W, Shi W, Yang Y, Bao L, Wang C, Wang T, Li H. A study on the internal vortex structure within a single-blade pump via numerical methods and particle image velocimetry experiments. Physics of Fluids. 2024;36:115130 doi:10.1063/5.0231983.

[14] Cui B, Li J, Zhang C, Zhang Y. Analysis of Radial Force and Vibration Energy in a Centrifugal Pump. Mathematical Problems in Engineering. 2020;1:6080942. doi:10.1155/2020/6080942

[15] Pei J, Dohmen HJ, Yuan SQ, Benra F-K. Investigation of unsteady flow-induced impeller oscillations of a single-blade pump under off-design conditions. Journal of Fluids and Structures. 2012;35:89-104. doi:10.1016/j.jfluidstructs.2012.08.005.

[16] Song X, Shi Y, Zheng K, Luo X. Pressure oscillations and radial forces for centrifugal pumps with single – or double-suction impellers. Journal of Mechanical Science and Technology. 2024;38(4):3009-3025. doi:10.1007/s12206-024-0521-2

[17] Ma S-B, Kim S, Kim J-H. Optimization Design of a Two-Vane Pump for Wastewater Treatment Using Machine-Learning-Based Surrogate Modeling. Processes. 2020;8:1170. doi:10.3390/pr8091170.

[18] Ren Y, Mo X, Yang B, Zheng S, Yang Y. Multi-objective optimization design of a sewage pump based on non-dominated sorting genetic algorithm III. Physics of Fluids. 2024;36:093342. doi:10.1063/5.0229088.

[19] Zhang H, Tang L, Zhao Y. Influence of Blade Profiles on Plastic Centrifugal Pump Performance. Advances in Materials Science and Engineering. 2020;2020:1-17. doi:10.1155/2020/6665520.

[20] ANSYS Fluent User's Guide, 2024R1

■